JACS
JOURNAL OF THE AMERICAN CHEMICAL SOCIETY

ARTICLE

pubs.acs.org/JACS

Improved Method for Kinetic Studies in Microreactors Using Flow Manipulation and Noninvasive Raman Spectrometry

Sergey Mozharov,[†] Alison Nordon,*[,†] David Littlejohn,*[,†] Charlotte Wiles,[‡] Paul Watts,[§] Paul Dallin,[∥] and John M. Girkin[⊥]

[†]WestCHEM, Department of Pure and Applied Chemistry and CPACT, University of Strathclyde, 295 Cathedral Street, Glasgow G1 1XL, United Kingdom

[‡]Chemtrix BV, Burgemeester Lemmensstraat 358, 6163JT Geleen, The Netherlands

[§]Department of Chemistry, The University of Hull, Cottingham Road, Hull HU6 7RX, United Kingdom

[∥]Clairet Scientific Ltd., 17/18 Scirocco Close, Moulton Park Industrial Estate, Northampton NN3 6AP, United Kingdom

[⊥]Department of Physics, University of Durham, South Road, Durham DH1 3LE, United Kingdom

Supporting Information

ABSTRACT: A novel method has been devised to derive kinetic information about reactions in microfluidic systems. Advantages have been demonstrated over conventional procedures for a Knoevenagel condensation reaction in terms of the time required to obtain the data (fivefold reduction) and the efficient use of reagents (tenfold reduction). The procedure is based on a step change from a low (e.g., 0.6 μL min^{-1}) to a high (e.g., 14 μL min^{-1}) flow rate and real-time noninvasive Raman measurements at the end of the flow line, which allows location-specific information to be obtained without the need to move the measurement probe along the microreactor channel. To validate the method, values of the effective reaction order n were obtained employing two different experimental methodologies. Using these values of n, rate constants k were calculated and compared. The values of k derived from the proposed method at 10 and 40 °C were 0.0356 ± 0.0008 mol$^{-0.3}$ dm$^{0.9}$ s^{-1} (n = 1.3) and 0.24 ± 0.018 mol$^{-0.1}$ dm$^{0.3}$ s^{-1} (n = 1.1), respectively, whereas the values obtained using a more laborious conventional methodology were 0.0335 ± 0.0032 mol$^{-0.4}$ dm$^{1.2}$ s^{-1} (n = 1.4) at 10 °C and 0.244 ± 0.032 mol$^{-0.3}$ dm$^{0.9}$ s^{-1} (n = 1.3) at 40 °C. The new approach is not limited to analysis by Raman spectrometry and can be used with different techniques that can be incorporated into the end of the flow path to provide rapid measurements.

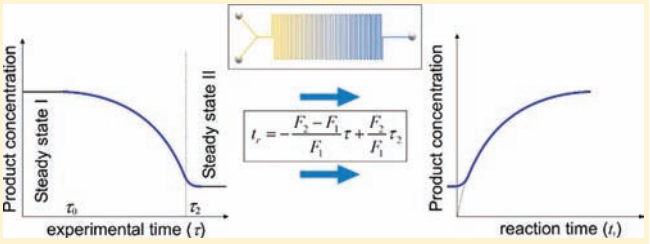

INTRODUCTION

Microfluidic devices have proven to be an exceptionally useful platform for a wide range of chemical applications[1,2] including the study of reaction kinetics, offering advantages over conventional batch experiments. For example, highly endothermic or exothermic reactions can be studied in virtually isothermal conditions owing to the efficient heat exchange in microchannels.[3] Kinetic studies of fast processes in flasks are complicated by the lack of homogeneity and relatively slow mixing that typify batch processes. In microchannels of special geometry, mixing can be as fast as 15 μs,[4] which is important for studies of extremely fast chemical reactions;[5,6] indeed, with time-resolved electrospray ionization mass spectrometry (ESI-MS) it is possible to directly study short-lived intermediates[7−9] with high time resolution. Another advantage of microreactors is the low consumption of chemicals, which is useful for rapid cost-effective catalyst screening.[3,10,11] Processes on a small scale are also easier to carry out in parallel, thus reducing analysis time and significantly increasing throughput.[12−14] It has been reported that the use of microreactors to study kinetic isotope effects provides better accuracy than alternative methods.[15−17] Furthermore, kinetic characterization of enzymes,[18,19] enzymatic assays,[20,21] and the study of enzymes immobilized within a microreactor[14,22−25] are among the most popular applications of microfluidics.

Obtaining relevant and timely analytical information for kinetic studies with microreactors can be challenging. Three categories of methodology are generally used based on extractive, in-line, or noninvasive analysis. For extractive procedures, a small portion of the fluid is removed from the microreactor for analysis by GC,[3] LC-MS,[25] or HPLC.[26] In-line analysis can be performed with an integrated sensor such as a microelectrode,[27,28] an on-chip microcoil NMR unit,[29] or an attenuated total reflection (ATR) crystal[30] for spectroscopic measurements. In-line analysis can also be carried out using an analyzer module directly attached to the microreactor for UV−visible spectrometry,[12,17,31] time-resolved ESI-MS,[8] or ATR-MIR spectrometry.[32] With

Received: November 14, 2010
Published: February 22, 2011

   dx.doi.org/10.1021/ja1102234 | J. Am. Chem. Soc. 2011, 133, 3601–3608

noninvasive analysis, where no physical contact with the sample is required,[33] information may be extracted from different locations on the microreactor.[34] Noninvasive methods offer a number of advantages, but so far only confocal optical techniques such as Raman spectrometry[34−36] and fluorescence spectrometry[37,38] have been applied successfully.

The type of flow manipulation[15] used in a microreactor often influences the preferred format of chemical analysis. The stopped flow approach[14,31,33] allows fast and frequent analysis of a stationary solution with either an in-line or a noninvasive sensor. With quenched flow, the reaction is terminated by introducing a quenching chemical to the fluidic path[12,39] or by using immobilized catalysts where the reaction stops automatically upon leaving the catalytic zone,[25] prior to extractive or in-line analysis. With continuous flow, in situ analysis can take place at the end of the microreactor[21,23] or at many different locations along the reactor by using a noninvasive probe.[34,36−38,40] When a continuous flow at a fixed flow rate is used, the fluid composition is constant over time at any location along the microchannel, which allows the opportunity to make measurements over longer periods to improve the signal-to-noise ratio with less sensitive methods of analysis, such as Raman spectrometry.

The use of noninvasive spectroscopic analysis at different locations along a microreactor is extremely useful in obtaining kinetic information about the reaction, optimizing reaction conditions in real time, and assisting with the rapid design of multistage microreactor assemblies. However, it is not always possible to have appropriate optical access to the whole flow path owing to the use of construction materials, reactor geometries, or operating conditions that prevent direct analysis of the content of the microreactor channels. In the present paper we describe a new procedure for the rapid acquisition of location-specific information about the reaction profile along a microreactor channel that involves analysis of the liquid as it exits the reactor. The procedure is based on flow manipulation and the use of rapid and frequent analytical measurements to generate a profile of the reaction within the reactor under selected temperature conditions. This approach allows much faster generation of kinetic data, such as reaction rate constants, than would be possible with conventional multiple-experiment procedures that use information derived only from a single point in the reaction profile. The new method is applied in this paper to study the kinetics of a Knoevenagel condensation reaction and involves the use of noninvasive Raman spectrometry with a novel optical interface optimized for microreactor measurements.[34]

METHOD

Model Microfluidic System. The model microreactor is schematically shown in Figure 1. The microfluidic pathway is presented as a tube with cross section s, length L, and total volume $V = sL$. The streams converge and mix in the microreactor junction ($x = 0$ in Figure 1). The mixing zone is assumed to be negligibly small compared to the total length of the reactor flow path. Similarly, the mixing time is considered small compared to the reaction time and can be neglected in the analysis. In the subsequent discussion, the term "flow rate" refers to the combined volumetric flow rate (F) of the reagents through the reactor.

An analyzer (in this case a Raman spectrometer with a noninvasive probe) collects data directly from the end of the microfluidic path ($x = L$ in Figure 1). The analysis time is minimal and the frequency of measurements is high. The cross section of the channel at the measurement zone must not be notably greater than that in the rest of the system

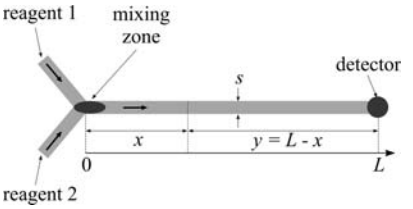

Figure 1. Schematic of the model microfluidic system. L is the length of the flow path, x is any distance along the flow path, and s is the channel cross section.

to prevent dispersion and the accompanying loss in compositional resolution that would result in an enlarged measurement cell.

Concept. The reaction initially takes place at a low flow rate (F_1) which ensures that the extent of the reaction changes significantly from the start to the end of the flow path. It is not necessary for the reaction to be complete by the end of the reactor; all that is required is that the selected analytical technique is sensitive enough to detect the change in the product or reactant concentrations along the flow path. With some reactors, analytical measurements can be made at various positions along the microreactor capillary, to allow production of a reaction profile from which kinetic information can be derived. However, this convention is not always possible owing to the design of reactor and materials of construction. In the new method, only one measurement position is required at the end of the reactor. After a sufficient period at low flow rate F_1, the flow is increased by about an order of magnitude to F_2. The high flow rate pushes the profile of reactants and products that has developed along the reactor capillary to the detector where many short-time interval analytical measurements are made. Knowing the magnitude of F_2, the time when it was applied, the dimensions of the flow path, and the times of all analytical measurements, it is possible to recreate the reaction profile that existed along the microreactor capillary when the flow rate was set at F_1. However, there are two important experimental aspects that need to be considered. First, the chemical reaction continues as the profile of reactants and products established at the lower flow rate is moved to the measurement zone at the higher flow rate. The extra reaction time will be least for the material right at the end of the reactor (closest to the measurement point) and greatest for the material at the start of the reactor. The variable extra reaction time has to be calculated and taken into account when trying to derive a true reaction profile corresponding to F_1. Second, the step increase in flow rate is never perfect. The system always needs some time to speed up to the higher flow rate. In addition, there is no guarantee that the flow system will respond to an abrupt increase in flow rate in the same way every time the procedure is repeated. The mathematical analysis provided below considers these issues and shows how to account for them theoretically as well as in a semiempirical way.

Mathematical Model. The reaction is initiated at flow rate F_1, and at a certain moment in time (τ_0), the higher flow rate F_2 is applied to the system as illustrated in Figure 2a, where τ is the experimental time. Figure 2b indicates the change in the product concentration recorded at the measurement point at the end of the reactor as a consequence of the increase in flow rate. If τ_0 is considered the zero point for changes to the system, three characteristic events will follow one another after the flow rate change: (i) after τ_1 seconds of speeding up the flow, the system stabilizes at flow rate F_2; the exact function $F(\tau)$ during this transitional period is uncertain; (ii) by τ_2 seconds, the initial part of the reaction profile established at flow rate F_1 (corresponding to position $x = 0$ in Figure 1 at time τ_0) reaches the detector; (iii) by τ_3 seconds, the new end-of-line concentration of product achieved at flow rate F_2 is established at the detector site.

During the time period from τ_2 to τ_3, the detector is exposed to the product formed from the liquid that entered the flow system during the

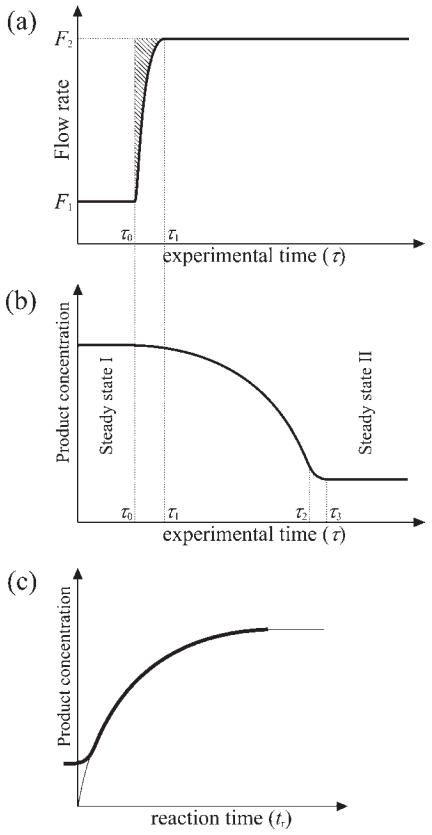

Figure 2. Changes in (a) flow rate and (b) the detected product concentration occurring during the proposed procedure and (c) the calculated kinetic curve.

flow rate change from τ_0 to τ_1 in Figure 2a. If the flow rate changed instantaneously, the parameters τ_2 and τ_3 would converge to a single point in Figure 2b.

By changing the flow rate from F_1 to F_2, the profile of the product formed along the flow path at F_1 is flushed rapidly to the analysis point at the end of the reactor where frequent measurements are made. Any distance x along the flow path (Figure 1) can be converted to a reaction time t_1 using eq 1:

$$t_1 = sx/F_1 \tag{1}$$

However, as it takes a finite time to move any point in the product profile to the measurement position, this extra reaction time, t_2, has to be considered in order to produce a kinetic curve like that illustrated in Figure 2c.

t_2 can be obtained from

$$t_2 = \tau - \tau_0 \tag{2}$$

So, the total reaction time, t_r, is

$$t_r = t_1 + t_2 \tag{3}$$

where t_2 is known from the experiment and t_1 can be derived from eq 1 as follows:

$$t_1 = \frac{sx}{F_1} = \frac{s(L-y)}{F_1} = \frac{V - sy}{F_1} \tag{4}$$

As illustrated in Figure 1, y is the distance from any position x to the measurement point at time τ_0; y can be calculated by integrating the flow rate function over time (from τ_0 to τ). For all experimental points obtained within $\tau_1 \le \tau \le \tau_2$, the following equation is true:

$$y(\tau) = \int_{\tau_0}^{\tau} \frac{F(\tau)}{s}\,d\tau = \frac{1}{s}\int_{\tau_0}^{\tau_1} F(\tau)\,d\tau + \frac{1}{s}\int_{\tau_1}^{\tau} F_2\,d\tau$$

$$= M + \frac{F_2}{s}(\tau - \tau_1) \tag{5}$$

The integral in eq 5 has been split into two terms in order to separate out the unknown part, labeled as M. After grouping the unknown parameters the following equation is derived:

$$y = \frac{F_2\tau}{s} - N \tag{6}$$

where

$$N = \frac{F_2\tau_1}{s} - M \tag{7}$$

The parameter N corresponds to the distance that the fluid travels in the channel during the period of uncertain flow rate, the shaded area in Figure 2a, that arises as a consequence of the flow rate change not being instantaneous.

Substitution of y in eq 4 with eq 6 yields the following solution for t_1:

$$t_1 = \frac{V - F_2\tau + sN}{F_1} \tag{8}$$

The solution for reaction time t_r is obtained from eqs 3 and 8:

$$t_r = -\frac{F_2 - F_1}{F_1}\tau + \frac{V + sN}{F_1} \tag{9}$$

With eq 9, the reaction time can be calculated for every experimental point, which allows generation of the kinetic curve of the reaction (Figure 2c).

Equation 9 suggests that the uncertainty of the system's response to the flow rate change does not affect the shape of the kinetic curve that is obtained within the boundaries in which eq 5 is correct ($\tau_1 \le \tau \le \tau_2$). Therefore, this uncertainty does not compromise the reliability of kinetic studies based on this strategy; it will only cause the recovered kinetic curve to shift along the time axis by $\Delta t = sN/F_1$. Although not essential for kinetic studies, knowing the magnitude of this shift can be useful for process optimization purposes.

Empirical Determination of Uncertain Parameters. Equation 9 does not hold for two regions of the original curve in Figure 2b: from τ_0 to τ_1 and from τ_2 to τ_3. Therefore, it is important to determine parameters τ_1, τ_2, and τ_3 in order to estimate the boundaries of these two uncertain zones. If the reaction mechanism or the rate equation is known, τ_2 can be estimated using a method based on this prior knowledge (see the Supporting Information). It can also be estimated graphically, as a point where the change in product concentration starts to decrease (Figure 2b); this is the method used in this study. τ_3 marks the first point where the concentration levels off. τ_1 cannot be directly derived from the curve shape, but it is possible to estimate it via other parameters as shown below.

Mathematically, τ_2 can be derived from eq 6 by substituting L for y and V for sL:

$$\tau_2 = \frac{V + sN}{F_2} \tag{10}$$

This equation provides an empirical solution for the uncertain parameter N:

$$N = \frac{F_2\tau_2 - V}{s} \tag{11}$$

With this solution eq 9 can be rewritten as follows:

$$t_r = -\frac{F_2 - F_1}{F_1}\tau + \frac{F_2}{F_1}\tau_2 \tag{12}$$

Determination of τ_1 is based on the following analysis. During the time period from τ_2 to τ_3, the detector is exposed to the portion of liquid

dx.doi.org/10.1021/ja1102234 |J. Am. Chem. Soc. 2011, 133, 3601–3608

that initially entered the system when the flow rate was uncertain (from τ_0 to τ_1). Consequently, the lengths of these two zones in the reactor capillary (corresponding to τ_0 to τ_1 and τ_2 to τ_3) are the same and equal to M (see eq 5). By time τ_2, the system has already been flowing at a stable higher flow rate F_2. Therefore, the period from τ_2 to τ_3 can be found from the definition of the volumetric flow rate, from which parameter M can be found as well:

$$\tau_3 - \tau_2 = \frac{Ms}{F_2} \tag{13}$$

$$M = \frac{(\tau_3 - \tau_2)F_2}{s} \tag{14}$$

A combination of eqs 7, 10, and 13 yields an empirical expression for τ_1:

$$\tau_1 = \tau_3 - \frac{V}{F_2} \tag{15}$$

Effect of Thermal Expansion. Equation 12, the main result of the present analysis, does not account for the effects of fluid expansion or contraction caused by a chemical reaction or temperature changes. Thermal expansion is likely to have a considerable effect. In fact, organic liquids are known to have especially high thermal expansion coefficients, with the volume changing by up to several percent for every 10 °C of temperature change. Microreactors are often kept at elevated or reduced temperatures during syntheses, whereas the temperature of the vials (syringes) from which reagents are delivered to the microreactor can be significantly different. However, the fluid temperature reaches the target value almost immediately upon entry into the microreactor owing to the extremely efficient heat transfer intrinsic to microfluidic systems. For the same reason, any heat liberated or absorbed during the chemical reaction is rapidly dissipated so that the temperature remains stable throughout the whole flow line. At higher temperatures, the liquid in the microreactor expands occupying more space and, therefore, flows faster than it would at a lower temperature. Thermal expansion is quantified by the volumetric coefficient of thermal expansion α_V.[41] In a flow system, the effect can be accounted for by introducing the effective flow rate, F_{eff}, which depends on α_V and the temperature difference ΔT:

$$F_{eff} = (1 + \alpha_V \Delta T)F \tag{16}$$

Derivation of eq 16 is given in the Supporting Information. Replacing the original flow rates F_1 and F_2 by the effective flow rates does not change eq 12; therefore, thermal expansion does not change the kinetic curve shape. But it does change eq 10 that defines τ_2:

$$\tau_2 = \frac{V + sN}{(1 + \alpha_V \Delta T)F_2} \tag{17}$$

If the thermal expansion coefficient for the reacting mixture is unknown, the effect of temperature can be considered as part of the total error contained in eq 17. With the latter approach it is sufficient to determine τ_2 from experimental data and enter the value obtained into eq 12.

For the liquids in this study, it was found that thermal expansion was 3.5 ± 0.5% over the temperature change from 10 to 40 °C; this was taken into account when calculating the maximum concentration of the product inside the microreactor as well as the residence time. Another factor that was taken into account was the reduction in volume that occurred when mixing the reagent steams, which was found to be 2.5 ± 0.5%.

EXPERIMENTAL SECTION

Reaction. The Knoevenagel condensation between ethyl cyanoacetate (**2**) and benzaldehyde (**1**) was selected as the model reaction (Scheme 1).

Scheme 1. Base-Catalyzed Knoevenagel Condensation between Ethyl Cyanoacetate and Benzaldehyde

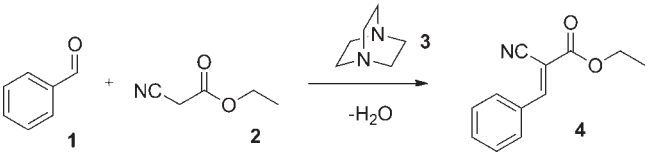

It was demonstrated experimentally that 100% conversion can be achieved at both temperatures used in the study. The absence of any notable side reactions was confirmed with GC-MS.

Solutions of the reagents were prepared according to the following procedure. Solution 1: 639.3 mg (6.02 mmol) of benzaldehyde (99+% m/m, Sigma Aldrich, Dorset, U.K.) and 67.4 mg (0.60 mmol) of 1,4-diazabicyclo[2.2.2]octane (**3**) (DABCO; 97+% m/m, Alfa Aesar, Heysham, U.K.) were diluted to 2 mL with methanol. Solution 2: 814.1 mg (7.20 mmol) of ethyl cyanoacetate (98+% m/m, Sigma Aldrich, Dorset, U.K.) was diluted with methanol to a total volume of 2 mL.

Microreactor Setup. The microreactor was designed to have a longer than normal path length and consisted of two glass microfluidic chips manufactured using wet-etching technology (University of Hull). The internal volumes of the chips were 8.6 and 14.6 μL, with average channel diameters of 125 and 160 μm, respectively. The chips were connected with a 50 cm long piece of PEEK tubing (i.d. 150 μm, part number 1572, Upchurch Scientific, U.S.) that was coiled and "sandwiched" between the chips. This arrangement was selected as it comprised a flow path length (1.9 m) typical of a multistage reactor assembly, which, although not required for the Knoevenagel condensation reaction, may be necessary for other reactions. Although it was considered important to evaluate the proposed methodology for longer flow paths than contained in a simple single chip configuration, the procedure is equally applicable to these reactors. It transpired that the longer total path length had an additional advantage in this study as it compensated for the instability of the pump at low flow rates.

The method assumes that the length of the mixing zone is negligibly small compared to the microreactor path length. In a previous study,[34] it was shown that small organic molecules need to travel approximately 6 cm in a 150 μm microchannel at 10 μL min^{-1} before they are mixed by diffusion. As the initial flow rate, F_1, was not more than 0.8 μL min^{-1}, the mixing zone was no more than 0.6 cm corresponding to less than 1% of the length of a typical microreactor chip with a flow path of 60−70 cm, and considerably less for the reactor assembly used.

Thermopaste (silicon-free heat sink grease; ITW Contamination Control, Denmark) was abundantly applied between the glass microreactors to ensure efficient heat exchange. The microreactor was glued to a Peltier element connected to a temperature controller (model 350, Newport Inc., U.S.). The aluminum heat sink was secured on an XY translation stage for precise positioning of the microreactor relative to the Raman probe. Reagents were delivered to the microreactor with a syringe pump (Kd Scientific) and 1 mL glass syringes (Gastight 1001, Hamilton, Switzerland). A schematic of the setup is given in Figure S1 in the Supporting Information.

Raman Spectrometry. The Raman probe (University of Strathclyde) was constructed according to the traditional backscattering design[42] and optimized for efficient signal collection from microchannels. The probe was focused on to the last line in the microreactor serpentine using a high-numerical-aperture (0.49) miniature aspheric lens. The design of the Raman probe used in this study has been described previously.[34] The Raman spectrometer (RXN-1, Kaiser Optical Systems Inc., U.S.) contained a 400 mW, 785 nm

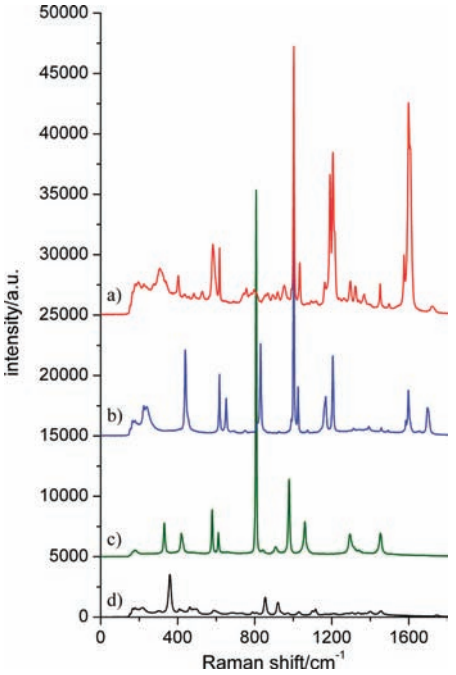

Figure 3. Offset Raman spectra of the individual compounds featured in the reaction: (a) ethyl 2-cyano-3-phenylacrylate (**4**), (b) benzaldehyde (**1**), (c) DABCO (**3**), and (d) ethyl cyanoacetate (**2**). An acquisition time of 0.5 s was employed.

laser, a Kaiser f/1.8 holographic imaging spectrograph, and a thermoelectrically cooled CCD camera. Care had to be taken to adjust the position of the probe to maintain focus when changing the temperature of the reaction. The microreactor channel moved out of focus by roughly 10 μm for every 10 °C temperature change owing to a combination of thermal expansion effects and a change in the refractive index of the borosilicate glass used to fabricate the microreactor.

Raman spectra of the product, reagents, and the catalyst obtained from a 5 mm cuvette are shown in Figure 3. The second most intense Raman peak of the product (ethyl 2-cyano-3-phenylacrylate (**4**)) located around 1600 cm^{-1} was selected for analysis, and the background-corrected peak area was calculated from 1564 to 1639 cm^{-1}. The intensity of the benzaldehyde band in this region is 13 times smaller than that of the product in equimolar solutions of the compounds. At early stages of the reaction, however, the benzaldehyde will make a notable contribution to the measured signal when the product concentration is low. In order to account for this interference, separate solutions containing ethyl 2-cyano-3-phenylacrylate or benzaldehyde in methanol at different concentrations were prepared and analyzed individually in the microreactor. The peak area signal from 1564 to 1639 cm^{-1} was calculated for each solution, and the information was used to build response curves for each compound. These curves were combined algebraically to account for the contribution of benzaldehyde using the condition that in the reaction mixture the total concentration of the two compounds is always equal to the initial concentration of benzaldehyde.

It was noted that temperature changes and also the chemical composition of the solution affected the area and shape of the Raman peak of the product. These effects resulted in less than a ±5% change in the peak area of the product, which was taken into account when calculating reaction conversion. Solutions containing the pure product and reagents dissolved in methanol in different concentrations were prepared and analyzed in the microreactor in order to build a calibration model that could be used to characterize the reaction quantitatively.

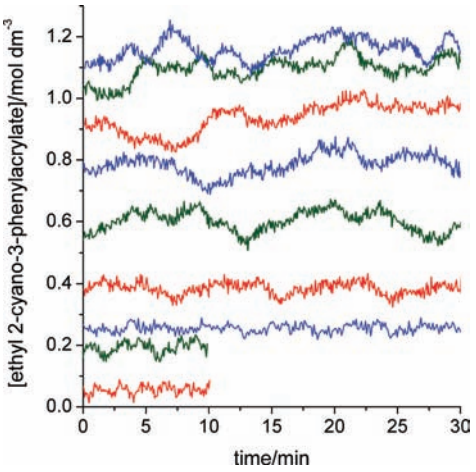

Figure 4. Change in the concentration of ethyl 2-cyano-3-phenylacrylate over time at different flow rates in method A (0.6, 0.8, 1.1, 1.6, 2.4, 4.0, 6.0, 8.0, and 20 μL min^{-1} corresponding to the lines from the top to the bottom of the figure).

Raman spectra were collected continuously throughout the kinetic experiments with an acquisition time of 2 s and 2 s delay time, giving 15 spectra per minute. The Holograms software (Kaiser Optical Systems Inc.) automatically recorded the time of each acquisition. Time conversion and data processing were performed in Matlab (Mathworks, U.S.).

Kinetic Experiments. The reaction was studied at two temperatures, 10 and 40 °C. The new method (B) was tested against a more conventional method (A) where several reactions were conducted at different flow rates (0.2−20 μL min^{-1}). At each flow rate in method A, there was a different residence time in the reactor so that the extent of the reaction was different by the time the liquid passed through the measurement zone at the end of the reactor. The analytical signal at each flow rate was averaged over 10−60 min to obtain the data points for the kinetic curve. A stabilization period, approximately 1.5 times the calculated residence time equivalent to the flow rate used, was allowed at each flow rate before measurements were initiated.

The new procedure, method B, involved initial stabilization of the flow system at a low flow rate F_1 followed by a step increase to F_2. Seven experiments were carried out at each temperature (10 and 40 °C) with different combinations of F_1 and F_2. The obtained data were processed using eq 12, and τ_2 values were derived graphically as described in the previous section.

RESULTS AND DISCUSSION

The Kinetic Model. A simple kinetic model was chosen to fit the experimental data and characterize and compare the obtained results, where the rate of reaction is proportional to the concentration of benzaldehyde to the power n, the effective reaction order.

The effective rate constant k can be found using the linearized rate equation for n-order reactions $(n \neq 1)$[43]

$$\frac{1}{[\mathrm{Bz}]_{t_r}^{n-1}} - \frac{1}{[\mathrm{Bz}]_0^{n-1}} = (n-1)kt_r \qquad (18)$$

where $[\mathrm{Bz}]_{t_r}$ is the concentration of benzaldehyde at the moment when the reaction time is t_r, and $[\mathrm{Bz}]_0$ is the initial concentration of benzaldehyde in the mixture, which was 1.538 ± 0.015 mol dm^{-3} at 10 °C and 1.485 ± 0.015 mol dm^{-3} at 40 °C.

In order to find the best linear fit of the data, the optimal values of parameters n and k must be found. If n is not known a priori, it

dx.doi.org/10.1021/ja1102234 |J. Am. Chem. Soc. 2011, 133, 3601–3608

has to be determined, although as outlined in the Supporting Information, n is likely to be between 1 and 2. For each experiment the value of n was found by plotting a series of curves (eq 18) using a range of n values from 1 to 2. The plot that had the highest value of the correlation coefficient R^2 was considered optimal, and the rate constant k was computed for this value of n.

Kinetic Analysis Method A. Figure 4 illustrates the change in the concentration of ethyl 2-cyano-3-phenylacrylate (product) over time obtained at different flow rates, based on the Raman signals recorded at the end of the microreactor. Considerable variation in the Raman signals (and hence derived concentrations) was observed at each flow rate owing to pumping instabilities. Five other pumps and different syringes were tested, and all the Raman signals demonstrated similar periodic fluctuations. Spectral noise is notably smaller than pumping-related noise.

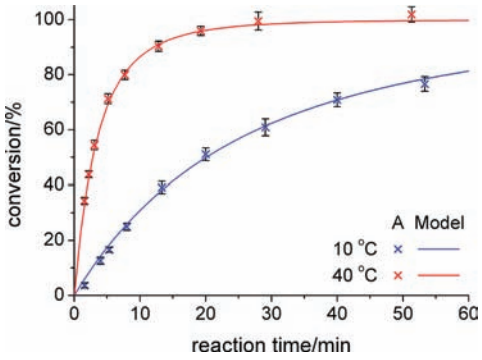

Figure 5. Kinetic curves obtained at 10 and 40 °C using method A based on Raman measurements of the product at different reaction times calculated from the flow rates mentioned in Figure 4. The solid lines represent the models with the optimal reaction order with respect to benzaldehyde (n = 1.4 at 10 °C and n = 1.3 at 40 °C).

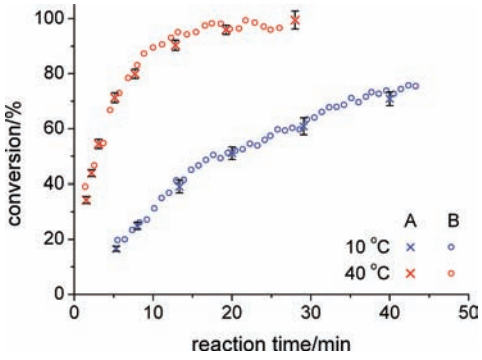

Figure 6. Kinetic curves computed using method B and flow rates F_1 and F_2 of 0.4 and 6 μL min^{-1} at 10 °C and 1.1 and 20 μL min^{-1} at 40 °C. The data obtained using method A are included for comparison.

To account for the pumping instability, the measured signal was averaged over 10−60 min at each flow rate, with longer times being used for the lower flow rates. By dividing the microreactor's internal volume by the flow rates used, the equivalent reaction times were calculated. The points in Figure 5 show the mean values of benzaldehyde conversion, derived from the Raman measurements, at the different reaction times for 10 and 40 °C. The error bars on the Y-axis are standard deviations that arise owing to variations in the measured signal caused by unstable pumping. The lines in Figure 5 represent the optimal kinetic models found for the experimental data as outlined in the previous section. The first seven experimental points at each temperature were used in the calculations to avoid the influence of the increased error observed for measurements for benzaldehyde close to 100% conversion.

As expected, reaction order values in the range from 1 to 2 produced the best fit at both temperatures, with n = 1.4 being optimal for the 10 °C curve and n = 1.3 for the 40 °C curve. Using these values of n, the rate constants derived from the data in Figure 5 were $(3.35 \pm 0.32) \times 10^{-2}$ mol$^{-0.4}$ dm$^{1.2}$ s^{-1} and $(24.4 \pm 3.2) \times 10^{-2}$ mol$^{-0.3}$ dm$^{0.9}$ s^{-1} for 10 and 40 °C, respectively.

Kinetic Analysis Method B. In method B, the reaction was allowed to proceed at a low flow rate for a period of time before increasing the flow to the higher rate. As the liquid exited the reactor at the higher flow rate, Raman measurements were made every 4 s to generate a reaction profile. The data were used to produce a kinetic curve, analogous to that derived with method A as illustrated in Figure 6 for flow rate combinations of 0.4 and 6 μL min^{-1} at 10 °C and 1.1 and 20 μL min^{-1} at 40 °C. This procedure was repeated for different combinations of F_1 and F_2 to investigate the influence of the choice of flow rates on the derived kinetic information. In each case the values of n and k were calculated using the same procedure as described for method A, and the results are shown in Table 1.

Although the dimensions of k depend on the values of n, the results in Table 1 suggest that the range of n values does not have

Table 1. Reaction Orders (n) and Rate Constants (k) Derived Using Method B for Different Combinations of Flow Rates (F_1 and F_2)[a]

10 °C				40 °C			
F_1, F_2 /μL min^{-1}	n	$k/10^{-2}$	$k/10^{-2}$ (n = 1.4)[b]	F_1, F_2 /μL min^{-1}	n	$k/10^{-2}$	$k/10^{-2}$ (n = 1.3)[b]
0.4, 6	1.6	3.49	3.49	1.1, 20	1.1	23.0	30.3
0.4, 6	1.1	3.54	3.53	1.1, 20	1.2	27.5	31.7
0.4, 6	1.3	3.49	3.49	0.6, 14	1.1	23.3	30.8
0.4, 6	1.3	3.72	3.73	1.6, 20	1.3	24.8	24.8
0.2, 4	1.4	3.50	3.50	2.4, 10	1.1	22.0	25.0
0.8, 8	1.1	3.59	3.59	1.1, 6	1.1	23.1	31.4
0.6, 6	1.1	3.57	3.60	1.1, 14	1.0	24.0	26.2
average	1.27 ± 0.19	3.56 ± 0.08	3.56 ± 0.09	average	1.13 ± 0.10	24.0 ± 1.8	28.6 ± 3.1

[a] The units of k have been omitted as they vary depending on the value of n. [b] Values of k calculated using the order of reaction at each temperature obtained with method A.

dx.doi.org/10.1021/ja1102234 |J. Am. Chem. Soc. 2011, 133, 3601–3608

a significant effect on the numerical value of k except for a few experiments at 40 °C. Table 1 also contains values of k calculated using the order of reaction at each temperature obtained with method A. In all cases the average values of n and k agree well with those found with method A. The higher errors associated with the data obtained at 40 °C occur because fewer experimental points were recorded owing to the faster reaction rate compared to that at 10 °C. Table 1 also shows that a range of flow rates F_1 and F_2 can be used with method B; similar results were obtained when the ratio F_2/F_1 ranged from 4 to 20.

As discussed earlier in the Method section, the change in flow rate is not instantaneous, and the effects of this are accounted for by the parameter τ_2. However, the accuracy of τ_2 is calculated from $\Delta\tau(F_2/F_1)$, where $\Delta\tau$ is the interval between consecutive measurements, and so can be reduced by increasing the frequency of Raman measurements.

Comparison of the Methods. Method B has a number of advantages over method A including the ability to derive a kinetic curve and associated parameters in a single experiment, lower consumption of reagents, and reduced experimental time (method B is roughly five times faster than method A). In method A accurate values of the microreactor volume and flow rates are essential for calculating reaction time, whereas method B requires only knowledge of the flow rate ratio F_2/F_1 (eq 12).

Method B also has advantages over stopped flow analysis, which does not provide spatial information along the flow path and also requires long measurement times especially for slow reactions. There are also some advantages in making measurements in a flowing liquid as with optical methods, photochemical effects or localized radiative heating, which can occur when analyzing stationary solutions, are avoided.

CONCLUSIONS

The proposed method offers advantages over conventional procedures for kinetic analysis and optimization of microfluidic reactions. The procedure makes it possible to extract location-specific information from the flow path without the need to access it directly with an optical probe. This approach enables processes to be analyzed in previously difficult situations where the microreactor is not transparent or optical access to the microchannels is not possible. The new approach is not limited to Raman spectroscopy and could be used with other analytical methods that can be integrated into the microchannel or an end-of-line measurement cell to rapidly extract chemical information. These alternative methods include, but are not limited to, electrochemical analysis, confocal fluorescence spectroscopy, transmission and ATR attachments for molecular absorption spectrometry, and refractive index sensors. The developed methodology offers the potential to increase the capabilities of these in-line measurement techniques in kinetic studies of microfluidic reactions.

ASSOCIATED CONTENT

Supporting Information. Description of an alternative method for estimation of τ_2, derivation of eq 16, schematic of the experimental setup, and derivation of the reaction order for the base-catalyzed Knoevenagel condensation reaction under two boundary conditions. This information is available free of charge via the Internet at http://pubs.acs.org.

AUTHOR INFORMATION

Corresponding Author
alison.nordon@strath.ac.uk; d.littlejohn@strath.ac.uk

ACKNOWLEDGMENT

S.M. was supported by the Scottish Funding Council, Centre for Process Analytics and Control Technology (CPACT) and the University of Strathclyde. The Royal Society is thanked for the award of a University Research Fellowship to A.N.

REFERENCES

(1) West, J.; Becker, M.; Tombrink, S.; Manz, A. *Anal. Chem.* **2008**, *80*, 4403.
(2) Dittrich, P. S.; Tachikawa, K.; Manz, A. *Anal. Chem.* **2006**, *78*, 3887.
(3) Cao, C.; Xia, G.; Holladay, J.; Jones, E.; Wang, Y. *Appl. Catal., A* **2004**, *262*, 19.
(4) Shastry, M. C. R.; Luck, S. D.; Roder, H. *Biophys. J.* **1998**, *74*, 2714.
(5) Park, S. H.; Shastry, M. C. R.; Roder, H. *Nat. Struct. Biol.* **1999**, *6*, 943.
(6) Kuwata, K.; Shastry, R.; Cheng, H.; Hoshino, M.; Batt, C. A.; Goto, Y.; Roder, H. *Nat. Struct. Biol.* **2001**, *8*, 151.
(7) Zechel, D. L.; Konermann, L.; Withers, S. G.; Douglas, D. J. *Biochemistry* **1998**, *37*, 7664.
(8) Rob, T.; Wilson, D. J. *J. Am. Soc. Mass Spectrom.* **2009**, *20*, 124.
(9) Simmons, D. A.; Konermann, L. *Biochemistry* **2002**, *41*, 1906.
(10) de Bellefon, C.; Tanchoux, N.; Caravieilhes, S.; Grenouillet, P.; Hessel, V. *Angew. Chem., Int. Ed.* **2000**, *39*, 3442.
(11) de Bellefon, C.; Pestre, N.; Lamouille, T.; Grenouillet, P.; Hessel, V. *Adv. Synth. Catal.* **2003**, *345*, 190.
(12) Bula, W. P.; Verboom, W.; Reinhoudt, D. N.; Gardeniers, H. *Lab Chip* **2007**, *7*, 1717.
(13) Duffy, D. C.; Gillis, H. L.; Lin, J.; Sheppard, N. F.; Kellogg, G. J. *Anal. Chem.* **1999**, *71*, 4669.
(14) Mao, H. B.; Yang, T. L.; Cremer, P. S. *Anal. Chem.* **2002**, *74*, 379.
(15) Zhou, X. Z.; Medhekar, R.; Toney, M. D. *Anal. Chem.* **2003**, *75*, 3681.
(16) Zhou, X. Z.; Toney, M. D. *J. Am. Chem. Soc.* **1998**, *120*, 13282.
(17) Xue, H.; Wu, X. W.; Huskey, W. P. *J. Am. Chem. Soc.* **1996**, *118*, 5804.
(18) Miyazaki, M.; Maeda, H. *Trends Biotechnol.* **2006**, *24*, 463.
(19) Urban, P. L.; Goodall, D. M.; Bruce, N. C. *Biotechnol. Adv.* **2006**, *24*, 42.
(20) Wang, J. *Electrophoresis* **2002**, *23*, 713.
(21) Hadd, A. G.; Raymond, D. E.; Halliwell, J. W.; Jacobson, S. C.; Ramsey, J. M. *Anal. Chem.* **1997**, *69*, 3407.
(22) Logan, T. C.; Clark, D. S.; Stachowiak, T. B.; Svec, F.; Frechet, J. M. J. *Anal. Chem.* **2007**, *79*, 6592.
(23) Seong, G. H.; Heo, J.; Crooks, R. M. *Anal. Chem.* **2003**, *75*, 3161.
(24) Srinivasan, A.; Bach, H.; Sherman, D. H.; Dordick, J. S. *Biotechnol. Bioeng.* **2004**, *88*, 528.
(25) Ono, Y.; Kitajima, M.; Daikoku, S.; Shiroya, T.; Nishihara, S.; Kanie, Y.; Suzuki, K.; Goto, S.; Kanie, O. *Lab Chip* **2008**, *8*, 2168.
(26) Matosevic, S.; Lye, G. J.; Baganz, F. *Biotechnol. Prog.* **2009**, *26*, 118.
(27) Wang, C.; Li, S. J.; Wu, Z. Q.; Xu, J. J.; Chen, H. Y.; Xia, X. H. *Lab Chip* **2010**, *10*, 639.
(28) Liu, A. L.; Zhou, T.; He, F. Y.; Xu, J. J.; Lu, Y.; Chen, H. Y.; Xia, X. H. *Lab Chip* **2006**, *6*, 811.
(29) Wensink, H.; Benito-Lopez, F.; Hermes, D. C.; Verboom, W.; Gardeniers, J. G. E.; Reinhoudt, D. N.; van den Berg, A. *Lab Chip* **2005**, *5*, 280.

(30) Sarov, Y.; Sarova, V.; Ivanov, T.; Ivanova, K.; Capek, I.; Rangelow, I. W. *Chem. Eng. J.* **2008**, *135*, S284.
(31) Hungerford, J. M.; Christian, G. D.; Ruzicka, J.; Giddings, J. C. *Anal. Chem.* **1985**, *57*, 1794.
(32) Carter, C. F.; Lange, H.; Ley, S. V.; Baxendale, I. R.; Wittkamp, B.; Goode, J. G.; Gaunt, N. L. *Org. Process Res. Dev.* **2010**, *14*, 393.
(33) Shende, C.; Maksymiuk, P.; Inscore, F.; Farquharson, S. *Proc. SPIE—Photon. Sens. Technol.* **2006**, *6371*, U45.
(34) Mozharov, S.; Nordon, A.; Girkin, J. M.; Littlejohn, D. *Lab Chip* **2010**, *10*, 2101.
(35) Leung, S. A.; Winkle, R. F.; Wootton, R. C. R.; deMello, A. J. *Analyst* **2005**, *130*, 46.
(36) Barnes, S. E.; Cygan, Z. T.; Yates, J. K.; Beers, K. L.; Amis, E. J. *Analyst* **2006**, *131*, 1027.
(37) Kerby, M. B.; Legge, R. S.; Tripathi, A. *Anal. Chem.* **2006**, *78*, 8273.
(38) Ristenpart, W. D.; Wan, J. D.; Stone, H. A. *Anal. Chem.* **2008**, *80*, 3270.
(39) Yamashita, K.; Miyazaki, M.; Nakamura, H.; Maedatt, H. *J. Phys. Chem. A* **2009**, *113*, 165.
(40) Gleason, N. J.; Carbeck, J. D. *Langmuir* **2004**, *20*, 6374.
(41) Graetzel, M.; Inelta, P. *The Bases of Chemical Thermodynamics*; Universal-Publishers: Parkland, FL, 2002; Vol. 1.
(42) Carrabba, M. M.; Rauh, R. D. U.S. Patent 5112127, 1992.
(43) Coker, A. K. *Modeling of Chemical Kinetics and Reactor Design*; Butterworth-Heinemann: Boston, MA, 2001.